

**$S = 1$  dimer system  $\text{K}_2\text{Ni}(\text{MoO}_4)_2$ : A candidate for magnon Bose-Einstein condensation**B. Lenz<sup>1,\*</sup>, B. Koteswararao<sup>2</sup>, S. Biermann<sup>3,4,5</sup>, P. Khuntia<sup>6,7</sup>, M. Baenitz<sup>7</sup> and S. K. Panda<sup>8,†</sup><sup>1</sup>*IMPMC, Sorbonne Université, CNRS, MNHN, 4 place Jussieu, F-75005 Paris, France*<sup>2</sup>*Department of Physics, Indian Institute of Technology Tirupati, Tirupati 517506, India*<sup>3</sup>*CPHT, CNRS, Ecole Polytechnique, IP Paris, F-91128 Palaiseau, France*<sup>4</sup>*Collège de France, 11 place Marcelin Berthelot, F-75005 Paris, France*<sup>5</sup>*Department of Physics, Division of Mathematical Physics, Lund University, Professorsgatan 1, SE-22363 Lund, Sweden*<sup>6</sup>*Department of Physics, Indian Institute of Technology Madras, Chennai 600036, India*<sup>7</sup>*Max-Planck Institute for Chemical Physics of Solids, D-01187 Dresden, Germany*<sup>8</sup>*Department of Physics, Bennett University, Greater Noida 201310, Uttar Pradesh, India*

(Received 18 August 2022; accepted 15 November 2022; published 29 November 2022)

Dimerized quantum magnets provide a unique possibility to investigate the Bose-Einstein condensation of magnetic excitations in crystalline systems at low temperature. Here, we model the low-temperature magnetic properties of the recently synthesized spin  $S = 1$  dimer system  $\text{K}_2\text{Ni}(\text{MoO}_4)_2$  and propose it as a candidate material for triplon and quintuplon condensation. Based on a first-principles analysis of its electronic structure, we derive an effective spin dimer model that we first solve within a mean-field approximation to refine its parameters in comparison to experiment. Finally, the model is solved by employing a numerically exact quantum Monte Carlo technique which leads to magnetic properties in good agreement with experimental magnetization and thermodynamic results. We discuss the emergent spin model of  $\text{K}_2\text{Ni}(\text{MoO}_4)_2$  in view of the condensation of magnetic excitations in a broad parameter regime. Finally, we comment on a geometrical peculiarity of the proposed model and discuss how it could host a supersolid phase upon structural distortions.

DOI: [10.1103/PhysRevB.106.L180408](https://doi.org/10.1103/PhysRevB.106.L180408)

**Introduction.** Low-dimensional quantum magnets provide a rich platform to study interesting magnetic phenomena in condensed matter physics due to their inherent strong quantum fluctuations. A variety of unusual ground states can be realized that sensitively depend on various parameters including dimensionality ( $D$ ), magnitude of the spin ( $S$ ), type of magnetic coupling, or range of correlations, just to name a few. Quantum materials thereby offer an ideal alternative route to investigate exotic phases of matter. A few prominent examples are superfluid and supersolid phases in Bose-Einstein condensates (BECs) [1,2], which are usually investigated under extreme conditions in ultracold atoms [3] or solid helium-4 [4,5].

In this regard, dimerized quantum magnets have sparked particular interest in recent years due to their inherent BEC of magnetic excitations [6,7]. These magnets offer the opportunity to study an effective gas of interacting bosons, whose particle number can be tuned by applying an external magnetic field:  $S = \frac{1}{2}$  spin dimers with antiferromagnetic (AFM) exchange coupling have a singlet ground state with a finite spin gap to its first excited state of spin  $S = 1$ . This state, however, becomes the ground state when applying a sufficiently strong external magnetic field—the magnetic moments order and an XY-antiferromagnetic phase is realized. By mapping the  $S = 1/2$  spins to hard-core bosons [8,9], it turns out that

the bosons can condense at this phase transition if the spin environment shows uniaxial symmetry [6,10]. For quantum magnets which fulfill this symmetry condition to a good approximation, the transition from a quantum paramagnetic to an XY-ordered state under an external magnetic field belongs to the BEC universality class.

The ground state properties and their excitations are extensively discussed for a plethora of  $S = \frac{1}{2}$  spin dimer materials, which include among others  $\text{TiCuCl}_3$  [11],  $\text{SrCu}_2(\text{BO}_3)_2$  [12],  $\text{BaCu}_2\text{Si}_2\text{O}_6$  [13],  $\text{Sr}_3\text{Cr}_2\text{O}_8$  [14], and  $\text{Ba}_3\text{Cr}_2\text{O}_8$  [15]. Many of the cited spin gap systems exhibit BEC-like excitations under applied magnetic fields or pressure [7,13,16–18]. On the other hand, very few materials with  $S = 1$  dimers exist in the literature [19,20], a famous example being  $\text{Ba}_3\text{Mn}_2\text{O}_8$  [19,21–26]. Interestingly, these systems show both triplet and quintuplet excitations: Whereas  $S = \frac{1}{2}$  spin dimer systems exhibit only triplet excitations, a second condensation into the  $|S = 2, S^z = 2\rangle$  state is possible for  $S = 1$  dimer systems in strong magnetic fields. Since the BEC properties heavily depend on dimensionality, lattice geometry, amount of disorder, and the nature of spin interactions [7], new  $S = 1$  dimer quantum magnets are sought after to investigate quintuplon condensation.

In this regard the recently rediscovered  $S = 1$  spin dimer system  $\text{K}_2\text{Ni}(\text{MoO}_4)_2$  [27,28] is promising: It has well-separated two-dimensional (2D) layers (*ac* planes) that consist of weakly coupled dimers formed by the magnetic ions of  $\text{Ni}^{2+}$  (see Fig. 1). The magnetic susceptibility and heat capacity results [27] indicate the presence of a spin gap in the

\*benjamin.lenz@sorbonne-universite.fr

†swarup.panda@bennett.edu.in

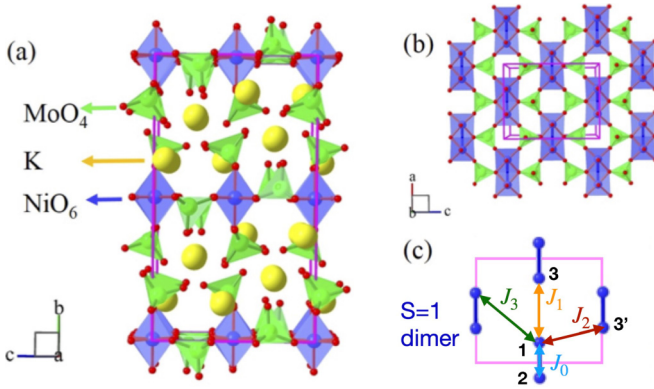


FIG. 1. (a) Crystal structure of  $\text{K}_2\text{Ni}(\text{MoO}_4)_2$ . The structure is composed of well-separated 2D layers ( $ac$  planes) of  $\text{Ni}^{2+}$  ( $S = 1$ ) atoms. (b) The  $ac$  plane is comprised of edge-sharing  $\text{NiO}_6$  octahedra, which are connected via  $\text{MoO}_4$  tetrahedra. (c) shows the arrangements of  $S = 1$  dimers in the 2D  $ac$  plane; the labels indicate different Ni-Ni spin exchange terms referred to in the text.

ground state and the magnetization shows a  $m = \frac{1}{2}$  plateau characteristic of spin-1 dimer systems.

In this Letter, we derive an effective magnetic model for  $\text{K}_2\text{Ni}(\text{MoO}_4)_2$  from first-principles calculations and refine it by comparing the computed magnetic properties with the experimental magnetization results. By estimating the interdimer spin exchange and mapping onto bosonic excitations, our theoretical modeling predicts superfluid phases of triplons and quintuplons in  $\text{K}_2\text{Ni}(\text{MoO}_4)_2$ . Moreover, we discuss the possibility of a supersolid phase upon structural distortions assuming a specific parametrization of the interdimer spin exchange. Our study motivates a more precise determination of the  $g$  tensor and spin exchange constants via electron spin resonance (ESR) and neutron scattering experiments in the future and suggests an investigation of  $\text{K}_2\text{Ni}(\text{MoO}_4)_2$  in the context of both triplon and quintuplon condensation.

**Model derivation from first principles.** In order to interpret the experimental results and to provide a microscopic understanding, we begin our theoretical analysis by carrying out *ab initio* simulations that allow us to derive an effective spin model.

First, we employ (non-spin-polarized) density functional theory (DFT) calculations [29,30] in the local density approximation (LDA) for the experimentally determined crystal structure. As can be seen from the band structure and densities of states (DOS) in Figs. 2(a) and 2(b) we find that the  $t_{2g}$  states are completely filled whereas  $e_g$  states are half filled, as expected for Ni ions in a  $2+$  charge state (a nominal  $d^8$  configuration). Our analysis shows that these bands around the Fermi level have predominant  $d_{x^2-y^2}$  and  $d_{yz}$  characters in the global reference frame [see Figs. 2(c) and 2(d)]. By constructing maximally localized Wannier functions [31] for these bands [see the inset of Fig. 2(b)] we obtain a low-energy tight-binding model. Effective hopping strengths between  $e_g$  orbitals [see Table I of the Supplemental Material (SM) [32]] indicate a strong dimer formation with much weaker interdimer coupling. In particular, the dimerization [e.g., between Ni atoms 1 and 2 in Fig. 1(c)] takes place between the  $x^2 - y^2$  orbitals, in agreement with the

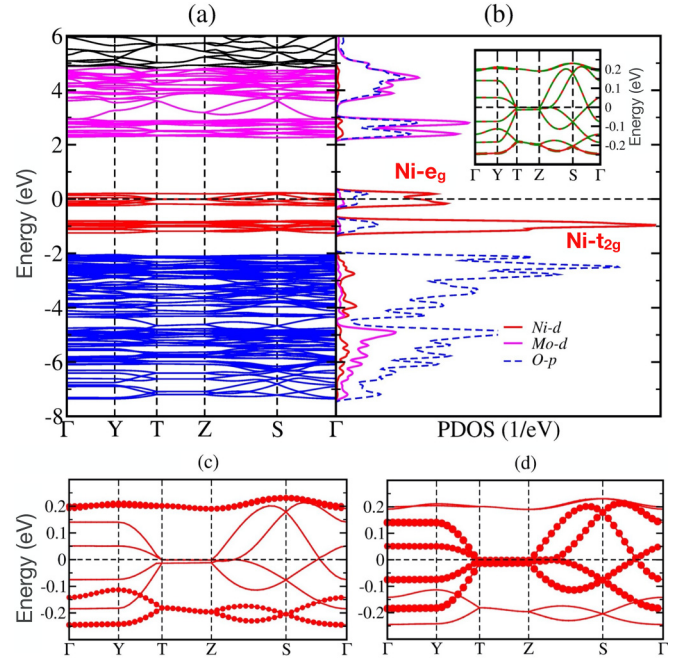


FIG. 2. (a) The band dispersion along various high-symmetry directions within LDA. (b) Partial density of states of Ni  $d$ , Mo  $d$ , and O  $p$  states for non-spin-polarized  $\text{K}_2\text{Ni}(\text{MoO}_4)_2$ . Fat-band representation of (c) Ni  $x^2 - y^2$  and (d)  $yz$  orbital character. The inset of (b) shows the Wannier-interpolated bands superimposed on the LDA bands. All orbitals are represented in the global reference frame.

pronounced bonding/antibonding splitting of the band structure in Fig. 2(c). This is consistent with fits of the magnetic susceptibility data of Ref. [27] (see SM [33]). These findings also suggest that the band structure of Fig. 2 should only be taken as an indication of the relevant electronic orbitals, since in reality  $\text{K}_2\text{Ni}(\text{MoO}_4)_2$  lies deep in the Mott phase. The half-filled  $x^2 - y^2$  and  $yz$  orbitals should thus be considered as localized states rather than band forming. Their low-energy physics is well described by an effective Heisenberg  $S = 1$  pseudospin model describing the coaligned spins of the half-filled Ni  $e_g$  orbitals. Its Hamiltonian is given by

$$\hat{H} = \sum_{i \neq j} J_{ij} \vec{S}_i \cdot \vec{S}_j,$$

where the indices  $i$  and  $j$  span the positions of the intrinsically magnetic ions in  $\text{K}_2\text{Ni}(\text{MoO}_4)_2$ , i.e., Ni, and negative (positive)  $J_{ij}$  denote (anti)ferromagnetic spin exchange constants. Since  $J_{ij}$  scales with the hopping terms  $t_{ij}$  as  $J_{ij} \sim (t_{ij,x^2-y^2}^2 + t_{ij,yz}^2)$  [32], the Wannierization of the electronic model suggests to limit the intersite spin exchange to nearest- and next-nearest neighbors in the  $ac$  plane [see Fig. 1(c)]. The Mott insulating limit of the electronic model also provides a clear hierarchy of the exchange constants, namely  $J_0 \gg J_1 \approx J_2$  [32]. Further constraints on the interdimer exchange constants  $J_1$ ,  $J_2$ , and  $J_3$  are obtained from a mean-field treatment of an effective pseudospin model, which amounts to fitting the linear regions of the measured magnetization curve under applied external magnetic field as discussed below.

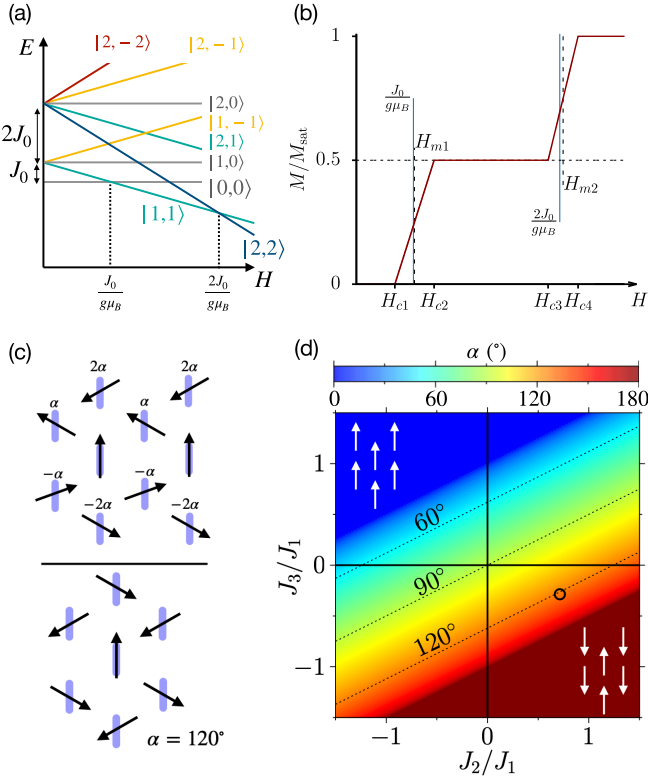


FIG. 3. (a) Energy level scheme of an isolated  $S = 1$  dimer: The ground state changes from singlet to triplet and finally to quintuplet as the applied magnetic field strength  $H$  is increased. (b) Schematic magnetization curve of the  $S = 1$  dimer lattice in mean-field theory. Linear slope regions are centered around  $H_{m1,2}$ . (c) The configurations of the transverse spin components in the magnetization slope regions  $\mathcal{I}_1$  and  $\mathcal{I}_2$  which are considered here.  $\alpha$  denotes the angle between the  $y$  axis and the transverse pseudospin of the dimer; the configuration  $\alpha = 120^\circ$  is close to the parametrization used here, which is indicated with a circle in (d). (d) The value of  $\alpha$  which minimizes the total energy as a function of  $J_2/J_1$  and  $J_3/J_1$  for  $J_0 = 33$  K.

To illustrate this approach, Fig. 3(a) sketches the characteristic energy level diagram of an isolated Ni dimer of  $\text{K}_2\text{NiMo}_2\text{O}_8$  as a function of applied magnetic field strength  $H$ . In zero field, the ground state has total spin  $S = 0$ , but at  $H_1 = \frac{J_0}{g\mu_B}$  the ground state changes to a  $S = 1$  triplet and for  $H > H_2 = \frac{2J_0}{g\mu_B}$  the dimer is in its  $S = 2$  quintuplet configuration. When treating the (weak) interdimer interactions in mean-field theory, the three configurations correspond to plateaus in the magnetization curve as sketched in Fig. 3(b): A magnetization plateau with half the saturated magnetization is reached for dimers in the triplet state. For large magnetic field strength, the dimer is finally in the quintuplet ( $|2, 2\rangle$ ) state and the magnetization reaches saturation. Due to the finite interdimer exchange terms, the linear magnetization regions around the transition points develop a finite slope. These regions are characterized by the critical field strengths  $H_{c1}$  to  $H_{c4}$  and the centers of each linear slope region,  $H_{m1}$ ,  $H_{m2}$ , can be compared to the critical field strengths extracted experimentally from  $dM/dH$ . In the following, we will briefly

revisit key aspects of the mean-field analysis, more technical details can be found in the SM [32].

**Mean-field calculations.** Following the technique outlined in the seminal paper by Uchida *et al.* [21], we start by identifying two regions,  $\mathcal{I}_1 = [H_{c1}, H_{c2}]$  and  $\mathcal{I}_2 = [H_{c3}, H_{c4}]$ , in which the ground state at zero temperature is only composed of the dimer spin states  $|0, 0\rangle$ ,  $|1, 1\rangle$  and  $|1, 1\rangle$ ,  $|2, 2\rangle$  respectively [see Fig. 3(a)]. In these regions we make the ansatz  $|\Psi\rangle = \otimes_i |\psi_i\rangle$  for the wave function, where

$$|\psi_i\rangle = \begin{cases} \cos(\theta_i)|0, 0\rangle + \sin(\theta_i)|1, 1\rangle e^{i\phi_i}, & H \in \mathcal{I}_1, \\ \cos(\theta_i)|1, 1\rangle + \sin(\theta_i)|2, 2\rangle e^{i\phi_i}, & H \in \mathcal{I}_2. \end{cases} \quad (1)$$

In order to investigate this region further, we rewrite the Hamiltonian in terms of dimer-spin operators and map onto the two lowest-lying states around the critical magnetic field strengths  $H_1$  ( $H_2$ ), which allows for a reformulation of the problem in terms of pseudospin-1/2 operators  $\hat{s}_i$ . In this new basis, the magnetization of the pseudospins amounts to a change from singlet to triplet (triplet to quintuplet) dimer states around  $H_1$  ( $H_2$ ). Thereby, we obtain a dimer-pseudospin model on a triangular lattice, where the pseudospin magnetization corresponds to the triplet (quintuplet) density.

In this description, the phases  $\phi_i$  have to be chosen such that they minimize the total energy of the system, which amounts to finding the optimal ordering of the transversal (XY) spin component of the antiferromagnet on a triangular lattice. To this end, we use the relative phases parametrized by an angle  $\alpha$  as sketched in Fig. 3(c), which leads to different possible relative spin orientations depending on the choice of  $J_1$ ,  $J_2$ , and  $J_3$  [see Fig. 3(d)].

Finally, the onsets of the linear slope regions of the magnetization can be expressed as

$$\begin{aligned} g\mu_B H_{c1} &= J_0 - \frac{8}{3}b, & g\mu_B H_{c3} &= 2J_0 - 2b + a, \\ g\mu_B H_{c2} &= J_0 + \frac{8}{3}b + a, & g\mu_B H_{c4} &= 2J_0 + 2b + 2a, \end{aligned} \quad (2)$$

where  $a = J_1 + 2J_2 + 4J_3$  and  $b = J_1 + (2J_3 - J_2)\cos\alpha - J_1\cos^2\alpha$ . Based on the measured values of the middle of the linear slope regions,  $H_{m1}$  and  $H_{m2}$ , as well as the critical field strengths  $H_{c1}$ ,  $H_{c2}$  determined from a linear fit of the magnetization curve, we estimate the spin exchange constants. Since precise information on the  $g_{ij}$  tensor is still missing, we assumed a constant  $g$  value of  $g = 2-2.1$ . Future ESR measurements of  $\text{K}_2\text{Ni}(\text{MoO}_4)_2$  would allow for a more precise refinement of the model. In particular the spin exchange  $J_3$  depends sensitively on the precise value of  $g$ , which has consequences for the possibility to host a super-solid phase as discussed below. In the following, we will use the parametrization obtained for  $g = 2$ , i.e.,  $J_0 = 33$  K,  $J_1 = 0.7$  K,  $J_2 = 0.5$  K, and  $J_3 = -0.2$  K. Treating the interdimer spin exchange in mean-field theory, we find the calculated magnetization curves in good qualitative agreement with the measurements of Ref. [27] [see Fig. 4(a)].

To cross-check this parametrization, we finally perform spin-polarized calculations within the local spin density approximation (LSDA) and LSDA+ $U$  (Hubbard  $U$ ) [34], which assume a static ordering of the spins. In both cases a magnetic state corresponding to an antiparallel spin ordering within and



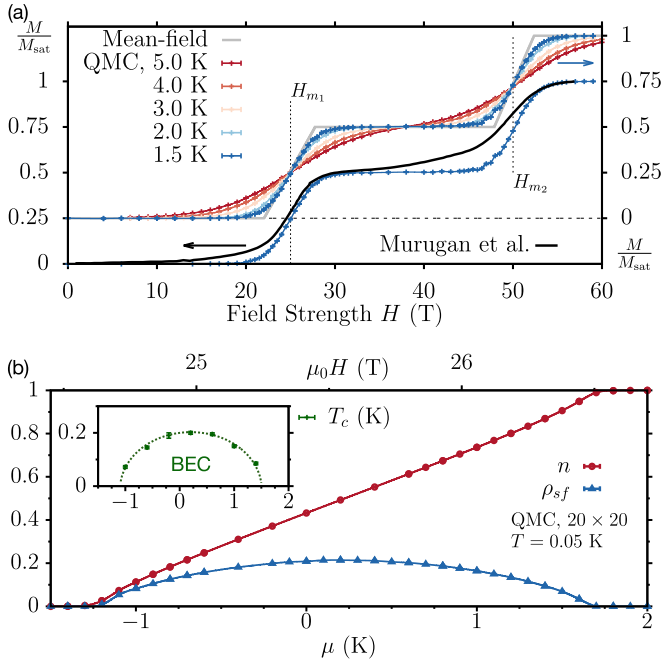


FIG. 4. (a) Magnetization as a function of applied magnetic field  $H$  as measured at  $T = 1.5$  K in Ref. [27] and as calculated from QMC simulations according to our model on a  $20 \times 20$  dimer lattice as well as mean-field curve. (b) Triplon density  $n$  and triplon superfluid stiffness  $\rho_{\text{sf}}$  of the corresponding hard-core boson model as a function of the chemical potential  $\mu$ . Inset: Finite-size extrapolated condensation temperature  $T_c$ . The lines are a guide to the eye.

between nearest-neighbor dimers is the lowest-energy state, consistent with the analysis in Ref. [27]. Effective exchange values  $J_{ij}$  extracted in a linear-response manner using the magnetic force theorem [35,36] confirm the parametrization qualitatively [32].

**Monte Carlo results.** The effective spin model with spin exchange terms  $J_0$ – $J_3$  on a triangular dimer lattice can be solved in a numerically exact way in two dimensions using quantum Monte Carlo (QMC) techniques. To this end, we use the worm QMC algorithm [37,38] as implemented in the ALPS package [39]. For the parameter regime used here [ $J_1, J_2$  antiferromagnetic,  $J_3$  ferromagnetic—see also Fig. 3(d)] there is no sign problem for the spin lattice, which is why the calculations are rather modest and can be converged with respect to the lattice size: The results are obtained for  $L \times L$  dimer lattices with up to  $L = 20$  and typically Monte Carlo sampling of  $\sim 10^6$  sweeps with 10% used for thermalization turn out to be sufficient. The calculations for  $J_3$  antiferromagnetic (see SM [32]), which introduces frustration via off-diagonal terms, need higher sampling.

Figure 4(a) shows the evolution of the calculated field-dependent magnetization curve for different temperatures. The mean-field result is recovered at low temperature and the curve at  $T = 1.5$  K is in good agreement with the experimental data of Ref. [27]. To illustrate the BEC of triplons, we plot in Fig. 4(b) the superfluid stiffness  $\rho_{\text{sf}}$  of the corresponding bosonic model around  $H_{c1} < H < H_{c2}$ . This model is obtained by mapping the triplon excitations onto hard-core bosons, which leads to a spatially anisotropic  $t$ - $V$  model on a

triangular lattice (see SM [32]). The triplon density smoothly increases from zero to one triplon per site when tuning the chemical potential across the parameter regime corresponding to the magnetic field strength  $H \in \mathcal{I}_1$ . The superfluid stiffness corresponds to the staggered in-plane magnetization  $m_{XY}$  of the spin model and indicates condensation of the triplon excitations below the critical temperature  $T_c$ . Since the superfluid density shows—in contrast to the triplon density—considerable finite-size effects, a proper scaling according to the Kosterlitz-Thouless recursion relations is applied [32,40]. The inset of Fig. 4(b) shows the condensation temperature  $T_c$  in the finite-size extrapolated limit, indicating the condensation of triplons around  $H_{m1}$  for  $T \lesssim 0.2$  K.

**Discussion and outlook.** We note first the qualitative agreement between the calculated magnetization curve and the measurements in Ref. [27]: The characteristic magnetization plateau at  $m = \frac{1}{2}$  between  $H_{c2}$  and  $H_{c3}$  is connected to the zero and saturation magnetization regions at small and high magnetic fields by linear slope regions. By adjusting the model parameters according to our mean-field analysis, we are able to reproduce the characteristic features of the curve such as the positions of the transitions and the size of the plateau even quantitatively.

Differences consist in an early onset of the linear slope region between 13 and 22 T, as well as in a very broad transition from the plateau to saturation magnetization. Although deviations in the high magnetic field might be related to the measurement in high fields, the finite magnetization in smaller magnetic fields  $\mu_0 H \sim 20$  T is a robust feature unrelated to uncertainties related to the experimental technique used. Our QMC simulations at finite temperature do also suggest that these deviations are not finite-temperature effects, since the linear part of the slope  $dM/dH$  close to  $H_c$  is correctly reproduced at  $T = 1.5$  K. Instead, we speculate that these small contributions to the magnetization curve could be linked to contaminations with the related compound  $\text{K}_2\text{Ni}_2(\text{MoO}_4)_3$  [41], which is a spin  $S = 1$  tetramer system that undergoes a Bose-Einstein condensation at smaller field strength.

The parametrization of our spin model can also be compared to estimates obtained from fitting the measured susceptibility data. Since the interdimer exchange constants are much smaller than the intradimer exchange, one can describe the spin susceptibility to a good approximation with a statistical ensemble of mean-field decoupled spin-1 dimers. This allows us to extract the intradimer exchange constant  $J_0$  as well as a mean-field correction due to the interdimer exchange (see SM [32]). Fitting the experimental data after subtracting impurity contributions yields an exchange constant of  $J_0 = 38.8$  K, which is a bit larger than our estimation of  $J_0 = 33$  K. This is not surprising since the determination of  $J_0$  from the susceptibility was shown to deviate from the one via inelastic neutron scattering in similar  $S = \frac{1}{2}$  dimer systems by roughly 13% [23,24]. In contrast to the analysis carried out in Ref. [27], we find the mean-field correction  $\lambda$  to be finite,  $\lambda = \frac{J_1 + 2J_2 - 4J_3}{Ng^2\mu_B^2} \approx 3$ , which is consistent with a small, but finite, interdimer spin exchange. However, one should note that the fit is rather insensitive to this quantity, which is why this technique does not allow for a precise determination of the effective interdimer exchange [24]. Finally, our estimate of  $J_0$

is also in agreement with the spin gap obtained from fitting the magnetic contribution to the specific heat [27] ( $\Delta \sim 38$  K).

The discussed Heisenberg model is the simplest model that qualitatively captures the essential features of the magnetization curve. A more realistic modeling should also include further terms such as single-ion anisotropy, the Dzyaloshinskii-Moriya interaction, and biquadratic terms. However, such a modelization requires precise knowledge of the different interaction parameters that enter the model and is beyond the scope of this Letter. It could become feasible once ESR and neutron scattering measurements on single crystals allow for determining the interdimer interactions with high precision. It should also be noted that adding a single-ion anisotropy term might change the size of the plateau region, but it would not qualitatively change the shape of the magnetization curve. In particular, calculations with reasonably sized single-ion anisotropies did not result in any additional linear slope regions in the magnetization curve that could explain the early onset of a nonzero magnetization found in experiment.

Finally, we note that the spin-1 Heisenberg model which captures the most prominent features of the system's magnetic properties includes a rather weak interdimer exchange term  $J_3$ , which sensitively depends on the precise value of the Landé  $g$  factor. Depending on  $g \in [2, 2.1]$  either ferro- or antiferromagnetic  $J_3$  leads to best agreement with the measured magnetization curves. In the latter case, the system would be a dimerized spin structure with *frustrated* interdimer couplings, which was identified in Ref. [2] as a crucial criterion for hosting an extended supersolid phase.

Here, however, due to the specific in-plane geometry of the spin dimers, we did not find supersolid behavior in the effective triplon and quintuplon models [32]. The reason lies

in the lack of interdimer spin frustration along the axis of the dimers. This is a conceptual difference to the  $S = 1$  dimer system Ba<sub>3</sub>Mn<sub>2</sub>O<sub>8</sub>, where the dimers are oriented perpendicular to the plane and which in principle allows for such phases. K<sub>2</sub>Ni(MoO<sub>4</sub>)<sub>2</sub> thereby not only offers the possibility to investigate Bose-Einstein condensation of triplons and quintuplons as a function of magnetic field, which has so far only been possible in few quantum magnets, but also renders K<sub>2</sub>Ni(MoO<sub>4</sub>)<sub>2</sub> a candidate to tune BEC without supersolid instability.

However, distortions of the crystal structure that lead to either in-plane rotations or out-of-plane buckling of the dimers would naturally induce additional frustrating interdimer spin terms that could then allow for a supersolid phase. The absence of anomalies in the specific heat and magnetic susceptibilities suggests a critical temperature for condensation below  $T = 1.5$  K, which is confirmed by the derived spin exchange strengths of our modelization. Overall, our results motivate the investigation of K<sub>2</sub>Ni(MoO<sub>4</sub>)<sub>2</sub> single crystals at low temperature in the future in the context of the realization of emergent states in quantum magnets with exotic magnetic excitations.

*Acknowledgments.* B.K. is thankful for support from a DST INSPIRE faculty award-2014 scheme. The figures showing crystal structures were created using the VESTA visualization software [42]. B.L. acknowledges computation time from the French grand équipement national de calcul intensif (GENCI) under Project No. A0110912043 and we thank the CPHT computer team for support. We thank R. Kumar and A. V. Mahajan for providing additional magnetic measurements. B.L. thanks Michele Casula for fruitful discussions on QMC and for drawing our attention to Ref. [40].

- 
- [1] N. Laflorencie and F. Mila, Quantum and Thermal Transitions Out of the Supersolid Phase of a 2D Quantum Antiferromagnet, *Phys. Rev. Lett.* **99**, 027202 (2007).
  - [2] P. Sengupta and C. D. Batista, Field-Induced Supersolid Phase in Spin-One Heisenberg Models, *Phys. Rev. Lett.* **98**, 227201 (2007).
  - [3] M. Greiner, O. Mandel, T. Esslinger, T. W. Hänsch, and I. Bloch, Quantum phase transition from a superfluid to a Mott insulator in a gas of ultracold atoms, *Nature (London)* **415**, 39 (2002).
  - [4] E. Kim and M. Chan, Probable observation of a supersolid helium phase, *Nature (London)* **427**, 225 (2004).
  - [5] E. Kim and M. H. W. Chan, Observation of superflow in solid helium, *Science* **305**, 1941 (2004).
  - [6] T. Giamarchi, C. Rüegg, and O. Tchernyshyov, Bose-Einstein condensation in magnetic insulators, *Nat. Phys.* **4**, 198 (2008).
  - [7] V. Zapf, M. Jaime, and C. D. Batista, Bose-Einstein condensation in quantum magnets, *Rev. Mod. Phys.* **86**, 563 (2014).
  - [8] T. Matsubara and H. Matsuda, A lattice model of liquid helium, I, *Prog. Theor. Phys.* **16**, 569 (1956).
  - [9] C. D. Batista and G. Ortiz, Algebraic approach to interacting quantum systems, *Adv. Phys.* **53**, 1 (2004).
  - [10] E. G. Batyev and L. S. Braginskii, Antiferromagnet in a strong magnetic field: analogy with Bose gas, *Sov. Phys. JETP* **60**, 781 (1984).
  - [11] A. Oosawa, M. Ishii, and H. Tanaka, Field-induced three-dimensional magnetic ordering in the spin-gap system, *J. Phys.: Condens. Matter* **11**, 265 (1999).
  - [12] H. Kageyama, K. Yoshimura, R. Stern, N. V. Mushnikov, K. Onizuka, M. Kato, K. Kosuge, C. P. Slichter, T. Goto, and Y. Ueda, Exact Dimer Ground State and Quantized Magnetization Plateaus in the Two-Dimensional Spin System SrCu<sub>2</sub>(BO<sub>3</sub>)<sub>2</sub>, *Phys. Rev. Lett.* **82**, 3168 (1999).
  - [13] M. Jaime, V. F. Correa, N. Harrison, C. D. Batista, N. Kawashima, Y. Kazuma, G. A. Jorge, R. Stern, I. Heinmaa, S. A. Zvyagin, Y. Sasago, and K. Uchinokura, Magnetic-Field-Induced Condensation of Triplons in Han Purple Pigment BaCuSi<sub>2</sub>O<sub>6</sub>, *Phys. Rev. Lett.* **93**, 087203 (2004).
  - [14] Y. Singh and D. C. Johnston, Singlet ground state in the spin- $\frac{1}{2}$  dimer compound Sr<sub>3</sub>Cr<sub>2</sub>O<sub>8</sub>, *Phys. Rev. B* **76**, 012407 (2007).
  - [15] T. Nakajima, H. Mitamura, and Y. Ueda, Singlet ground state and magnetic interactions in new spin dimer system Ba<sub>3</sub>Cr<sub>2</sub>O<sub>8</sub>, *J. Phys. Soc. Jpn.* **75**, 054706 (2006).
  - [16] T. Nikuni, M. Oshikawa, A. Oosawa, and H. Tanaka, Bose-Einstein Condensation of Dilute Magnons in TiCuCl<sub>3</sub>, *Phys. Rev. Lett.* **84**, 5868 (2000).
  - [17] C. Rüegg, N. Cavadini, A. Furrer, H.-J. Güdel, K. Krämer, H. Mutka, A. Wildes, K. Habicht, and P. Vorderwisch, Bose-Einstein condensation of the triplet states in the magnetic insulator TiCuCl<sub>3</sub>, *Nature (London)* **423**, 62 (2003).

- [18] A. A. Aczel, Y. Kohama, M. Jaime, K. Ninios, H. B. Chan, L. Balicas, H. A. Dabkowska, and G. M. Luke, Bose-Einstein condensation of triplons in  $\text{Ba}_3\text{Cr}_2\text{O}_8$ , *Phys. Rev. B* **79**, 100409(R) (2009).
- [19] M. Uchida, H. Tanaka, M. Bartashevich, and T. Goto, Singlet ground state and magnetization plateaus in  $\text{Ba}_3\text{Mn}_2\text{O}_8$ , *J. Phys. Soc. Jpn.* **70**, 1790 (2001).
- [20] Y. Hosokoshi, Y. Nakazawa, K. Inoue, K. Takizawa, H. Nakano, M. Takahashi, and T. Goto, Magnetic properties of low-dimensional quantum spin systems made of stable organic biradicals PNNNO,  $\text{F}_2\text{PNNNO}$ , and PIMNO, *Phys. Rev. B* **60**, 12924 (1999).
- [21] M. Uchida, H. Tanaka, H. Mitamura, F. Ishikawa, and T. Goto, High-field magnetization process in the  $S = 1$  quantum spin system  $\text{Ba}_3\text{Mn}_2\text{O}_8$ , *Phys. Rev. B* **66**, 054429 (2002).
- [22] H. Tsujii, B. Andraka, M. Uchida, H. Tanaka, and Y. Takano, Specific heat of the  $S = 1$  spin-dimer antiferromagnet  $\text{Ba}_3\text{Mn}_2\text{O}_8$  in high magnetic fields, *Phys. Rev. B* **72**, 214434 (2005).
- [23] M. B. Stone, M. D. Lumsden, S. Chang, E. C. Samulon, C. D. Batista, and I. R. Fisher, Singlet-Triplet Dispersion Reveals Additional Frustration in the Triangular-Lattice Dimer Compound  $\text{Ba}_3\text{Mn}_2\text{O}_8$ , *Phys. Rev. Lett.* **100**, 237201 (2008).
- [24] E. C. Samulon, Y.-J. Jo, P. Sengupta, C. D. Batista, M. Jaime, L. Balicas, and I. R. Fisher, Ordered magnetic phases of the frustrated spin-dimer compound  $\text{Ba}_3\text{Mn}_2\text{O}_8$ , *Phys. Rev. B* **77**, 214441 (2008).
- [25] E. C. Samulon, Y. Kohama, R. D. McDonald, M. C. Shapiro, K. A. Al-Hassanieh, C. D. Batista, M. Jaime, and I. R. Fisher, Asymmetric Quintuplet Condensation in the Frustrated  $S = 1$  Spin Dimer Compound  $\text{Ba}_3\text{Mn}_2\text{O}_8$ , *Phys. Rev. Lett.* **103**, 047202 (2009).
- [26] E. C. Samulon, K. A. Al-Hassanieh, Y.-J. Jo, M. C. Shapiro, L. Balicas, C. D. Batista, and I. R. Fisher, Anisotropic phase diagram of the frustrated spin dimer compound  $\text{Ba}_3\text{Mn}_2\text{O}_8$ , *Phys. Rev. B* **81**, 104421 (2010).
- [27] G. S. Murugan, K. R. Babu, R. Sankar, W. T. Chen, I. P. Muthuselvam, S. Chattopadhyay, and K.-Y. Choi, Magnetic and structural dimer networks in layered  $\text{K}_2\text{Ni}(\text{MoO}_4)_2$ , *Phys. Rev. B* **103**, 024451 (2021).
- [28] R. Klevtsova and P. Klevtsov, Crystal structure of double molybdate  $\text{K}_2\text{Ni}(\text{MoO}_4)_2$ , *Kristallografiya* **23**, 261 (1978).
- [29] P. Hohenberg and W. Kohn, Inhomogeneous electron gas, *Phys. Rev.* **136**, B864 (1964).
- [30] R. O. Jones and O. Gunnarsson, The density functional formalism, its applications and prospects, *Rev. Mod. Phys.* **61**, 689 (1989).
- [31] N. Marzari, A. A. Mostofi, J. R. Yates, I. Souza, and D. Vanderbilt, Maximally localized Wannier functions: Theory and applications, *Rev. Mod. Phys.* **84**, 1419 (2012).
- [32] See Supplemental Material at <http://link.aps.org/supplemental/10.1103/PhysRevB.106.L180408> for technical details of the *ab initio* calculations, the mean-field analysis and the derivation of the hard-core boson model, which includes Refs. [43–62].
- [33] Details of the fit and our mean-field estimate of the interdimer coupling, which is slightly different from Ref. [27], can be found in the Supplemental Material [32].
- [34] V. I. Anisimov, F. Aryasetiawan, and A. I. Lichtenstein, First-principles calculations of the electronic structure and spectra of strongly correlated systems: the LDA+U method, *J. Phys.: Condens. Matter* **9**, 767 (1997).
- [35] A. Liechtenstein, M. Katsnelson, V. Antropov, and V. Gubanov, Local spin density functional approach to the theory of exchange interactions in ferromagnetic metals and alloys, *J. Magn. Magn. Mater.* **67**, 65 (1987).
- [36] M. I. Katsnelson and A. I. Lichtenstein, First-principles calculations of magnetic interactions in correlated systems, *Phys. Rev. B* **61**, 8906 (2000).
- [37] N. Prokof'ev, B. Svistunov, and I. Tupitsyn, Worm algorithm in quantum Monte Carlo simulations, *Phys. Lett. A* **238**, 253 (1998). Exact, complete, and universal continuous-time world-line Monte Carlo approach to the statistics of discrete quantum systems, *J. Exp. Theor. Phys.* **87**, 310 (1998).
- [38] M. Troyer, F. Alet, S. Trebst, and S. Wessel, Non-local updates for quantum Monte Carlo simulations, in *The Monte Carlo Method in the Physical Sciences: Celebrating the 50th Anniversary of the Metropolis Algorithm*, edited by J. E. Gubernatis, AIP Conf. Proc. Vol. 690 (AIP, Melville, NY, 2003), p. 156.
- [39] A. Albuquerque, F. Alet, P. Corboz, P. Dayal, A. Feiguin, S. Fuchs, L. Gamper, E. Gull, S. Gürtler, A. Honecker, R. Igarashi, M. Körner, A. Kozhevnikov, A. Läuchli, S. Manmana, M. Matsumoto, I. McCulloch, F. Michel, R. Noack, G. Pawłowski *et al.*, The ALPS project release 1.3: Open-source software for strongly correlated systems, *J. Magn. Magn. Mater.* **310**, 1187 (2007); B. Bauer, L. T. Carr, H. G. Evertz, A. E. Feiguin, J. Freire, S. Fuchs, L. Gamper, J. Gukelberger, E. Gull, S. Guertler, A. Hehn, R. Igarashi, S. V. Isakov, D. Koop, P. N. Ma, P. Mates, H. Matsuo, O. Parcollet, G. Pawłowski, J. D. Picon *et al.*, The ALPS project release 2.0: open source softsoft for strongly correlated Systems, *J. Stat. Mech.: Theory Exp.* (2011) P05001.
- [40] D. M. Ceperley and E. L. Pollock, Path-integral simulation of the superfluid transition in two-dimensional  $^4\text{He}$ , *Phys. Rev. B* **39**, 2084 (1989).
- [41] B. Koteswararao, P. Khuntia, R. Kumar, A. V. Mahajan, A. Yogi, M. Baenitz, Y. Skourski, and F. C. Chou, Bose-Einstein condensation of triplons in the  $S = 1$  tetramer antiferromagnet  $\text{K}_2\text{Ni}_2(\text{MoO}_4)_3$ : A compound close to a quantum critical point, *Phys. Rev. B* **95**, 180407(R) (2017).
- [42] K. Momma and F. Izumi, VESTA3 for three-dimensional visualization of crystal, volumetric and morphology data, *J. Appl. Crystallogr.* **44**, 1272 (2011).
- [43] P.-O. Löwdin, A note on the quantum-mechanical perturbation theory, *J. Chem. Phys.* **19**, 1396 (1951).
- [44] J. M. Wills, O. Eriksson, M. Alouni, and D. L. Price, *Electronic Structure and Physical Properties of Solids: The Uses of the LMTO Method* (Springer, Berlin, 2000).
- [45] Y. O. Kvashnin, O. Grånäs, I. Di Marco, M. I. Katsnelson, A. I. Lichtenstein, and O. Eriksson, Exchange parameters of strongly correlated materials: Extraction from spin-polarized density functional theory plus dynamical mean-field theory, *Phys. Rev. B* **91**, 125133 (2015).
- [46] A. I. Liechtenstein, V. I. Anisimov, and J. Zaanen, Density-functional theory and strong interactions: Orbital ordering in Mott-Hubbard insulators, *Phys. Rev. B* **52**, R5467(R) (1995).
- [47] P. E. Blöchl, Projector augmented-wave method, *Phys. Rev. B* **50**, 17953 (1994).

- [48] G. Kresse and J. Furthmüller, Efficient iterative schemes for *ab initio* total-energy calculations using a plane-wave basis set, *Phys. Rev. B* **54**, 11169 (1996).
- [49] P. Blaha, K. Schwarz, P. Sorantin, and S. Trickey, Full-potential, linearized augmented plane wave programs for crystalline systems, *Comput. Phys. Commun.* **59**, 399 (1990).
- [50] J. M. Wills and B. R. Cooper, Synthesis of band and model Hamiltonian theory for hybridizing cerium systems, *Phys. Rev. B* **36**, 3809 (1987).
- [51] O. K. Andersen, Linear methods in band theory, *Phys. Rev. B* **12**, 3060 (1975).
- [52] S. K. Panda, H. Jiang, and S. Biermann, Pressure dependence of dynamically screened Coulomb interactions in NiO: Effective Hubbard, Hund, intershell, and intersite components, *Phys. Rev. B* **96**, 045137 (2017).
- [53] J. Rodríguez-Carvajal, Recent advances in magnetic structure determination by neutron powder diffraction, *Phys. B: Condens. Matter* **192**, 55 (1993).
- [54] A. A. Mostofi, J. R. Yates, Y.-S. Lee, I. Souza, D. Vanderbilt, and N. Marzari, wannier90: A tool for obtaining maximally-localised Wannier functions, *Comput. Phys. Commun.* **178**, 685 (2008).
- [55] J. Kuneš, R. Arita, P. Wissgott, A. Toschi, H. Ikeda, and K. Held, Wien2wannier: From linearized augmented plane waves to maximally localized Wannier functions, *Comput. Phys. Commun.* **181**, 1888 (2010).
- [56] M. Boninsegni and N. Prokof'ev, Supersolid Phase of Hard-Core Bosons on a Triangular Lattice, *Phys. Rev. Lett.* **95**, 237204 (2005).
- [57] S. Wessel and M. Troyer, Supersolid Hard-Core Bosons on the Triangular Lattice, *Phys. Rev. Lett.* **95**, 127205 (2005).
- [58] D. Heidarian and K. Damle, Persistent Supersolid Phase of Hard-Core Bosons on the Triangular Lattice, *Phys. Rev. Lett.* **95**, 127206 (2005).
- [59] R. G. Melko, A. Paramekanti, A. A. Burkov, A. Vishwanath, D. N. Sheng, and L. Balents, Supersolid Order from Disorder: Hard-Core Bosons on the Triangular Lattice, *Phys. Rev. Lett.* **95**, 127207 (2005).
- [60] J.-Y. Gan, Effects of frustration on the anisotropic triangular lattice bosons, *Phys. Rev. B* **78**, 014513 (2008).
- [61] X.-F. Zhang, S. Hu, A. Pelster, and S. Eggert, Quantum Domain Walls Induce Incommensurate Supersolid Phase on the Anisotropic Triangular Lattice, *Phys. Rev. Lett.* **117**, 193201 (2016).
- [62] S. A. Zvyagin, J. Wosnitza, J. Krzystek, R. Stern, M. Jaime, Y. Sasago, and K. Uchinokura, Spin-triplet excitons in the  $S = \frac{1}{2}$  gapped antiferromagnet  $\text{BaCuSi}_2\text{O}_6$ : Electron paramagnetic resonance studies, *Phys. Rev. B* **73**, 094446 (2006).